MIrai Radar Data: DYNAMO Legacy Collection

Rutledge, Steven   rutledge@atmos.colostate.edu

Professor, Dept. of Atmospheric Science, Colorado State University
Campus Delivery 1371, Fort Collins, CO 80523-1371.

Hein, Paul F.   hein@atmos.colostate.edu

Research Associate, Dept. of Atmospheric Science, Colorado State University
Campus Delivery 1371, Fort Collins, CO 80523-1371.

Dolan, Brenda   bdolan@atmos.colostate.edu

Research Scientist, Dept. of Atmospheric Science, Colorado State University
Campus Delivery 1371, Fort Collins, CO 80523-1371.

Powell, Scott W.   spowell@atmos.colostate.edu
NOAA C&GC Postdoctoral Fellow, Dept. of Atmospheric Science, Colorado State University
Campus Delivery 1371, Fort Collins, CO 80523-1371

To cite the data in publications:
Rutledge, Steven, Paul F. Hein, Brenda Dolan, Scott W. Powell (2018), MIrai Radar Data: DYNAMO Legacy Collection. [Data Access Date] [Reference Number]

1. Data Set Overview:

This document describes the data collected by ship radar on the MIrai during DYNAMO and the post-processing that was performed on it. It also describes several products that were derived from it: raintype maps, rainrate maps and echo top heights.

Time period: 25 September – 26 October 2011 (Leg 1) and 29 October 2011 – 1 December 2011 (Leg 2), continuous 24 hour coverage

Physical location: The MIrai ship with its radar was stationed at 8°S and 80.5°E. There are a small number of times at the start and end of each leg when the ship was not on station. They arrived on station on 30 September 2011 and departed station on 24 October 2011 for Leg 1, and for Leg 2 they arrived on station on 30 October 2011 and departed station on 28 November 2011.

Data source: Data collected by the Mirai C-band radar

2. Instrument Description

MIrai C-Band Doppler Radar

Frequency	5290 MHz
Beam width	1.4°
Gate Spacing	250 m
PPI Azimuthal Spacing	1°
Maximum Unambiguous Range	160 km
Nyquist Velocity	51.03 ms^{-1}

3. Data Collection and Processing

The MIrai radar operated on a 10-min scan cycle, starting at minute 0, 10, 20… of every hour, for six total scan cycles per hour with PPI and RHI scans. Only the PPI scans are used in these products. The files went through a quality control process and an attenuation correction. Procedures for such can be found in Dolan et al. (2017).

Those files were interpolated using NCAR's Radx2Grid application (https://ral.ucar.edu/projects/titan/docs/radial_formats/radx.html) to a 321 km x 321 km grid ranging from 0.5-20 km in altitude with horizontal and vertical grid spacings of 1km and 0.5 km, respectively.

Each field in each volume was interpolated separately so that for each volume time, there are two separate gridded files, one for each field in the table below.

Interpolated (Legacy) Field Name	cfradial Field Name
REFL	AZ
WIDTH	SW

Derived Products

In addition to the radar data itself, there are three derived products associated with each SUR volume – rain type map, rain rate map, echo top heights. All of them are based on the gridded radar data set. The rain type and rain rate maps are based on the 2.5 km level of the gridded radar data and are described in "DYNAMO Legacy Rainfall Products" (Dolan et al., 2017)

Not mentioned specifically in that paper are the input parameters used for rain type calculations. The algorithm is described in [Powell et al., 2016]

Input Parameter	Value Used
minZdiff	20
deepcoszero	40
shallowconvmin	28
truncZconvthres	38
dBZformaxconvradius	43
weakechothres	7
backgrndradius	5
maxconvRadius	10
minsize	8
startslope	50
maxsize	2000

4. Data Format
   a. The DATA are in CF-compliant NetCDF format.
   b. The file naming convention is **radar.ship.MIrai.<variable>.YYYYMMDD.HHMMSS.nc**.

Radar Products

Radar Reflectivity
File naming: "radar.ship.mIrai.refl.<yyyymmdd>.<hhmmss>.nc"

Description: Radar reflectivity interpolated to fixed grids with 1 km horizontal resolution and heights from 0.5 km to 20.0 km.

Variable Name: "REFL"

Radar Spectrum Width
File naming: "radar.ship.mIrai.width.<yyyymmdd>.<hhmmss>.nc"

Description: Radar spectrum width interpolated to fixed grids with 1 km horizontal resolution and heights from 0.5 km to 20.0 km.

Variable Name: "WIDTH"

Echo Tops
File naming: "radar.ship.mIrai.echotops.<yyyymmdd>.<hhmmss>.nc"

Description: Radar echo top in km from the gridded radar reflectivity product. Radar reflectivity thresholds include 0, 10, 20, 30, 40 and 50 dBZ.

Variable Name: "echo_top"

Rain Rates
File naming: "radar.ship.mIrai.rainrate.<yyyymmdd>.<hhmmss>.nc"

Description: Radar estimated rain rates from the gridded radar reflectivity product at the 2.5 km level. Minimum and maximum estimates of rain rates are provided in separate variables to account for measurement error and the uncertainty in the reflectivity-rain rate relationships. Rain_rate is the best estimate, and rain_rate_min and rain_rate_max are arrived at as described in Dolan et al. (2017).

Variable Name: "rain_rate", "rain_rate_min", "rain_rate_max"

Rain Type
File naming: "radar.ship.mIrai.raintype.<yyyymmdd>.<hhmmss>.nc"

Description: Rain type classifications from the gridded radar reflectivity product at the 2.5 km level. The determination of rain type follows the method described in Powell et al. (2016).

Variable Name: "rain_type"

5. Data Remarks

The data can be accessed using the myriad of software that is able to interact with NetCDF format files, including ncdump, ncview, Matlab, Python, IDL, and NCL. Consult the user help system within each software package.

See attached "DYNAMO Legacy Rainfall Products" (Dolan et al., 2017) for more information on processing.

6. References

Dolan, B., P. Hein, S. Rutledge, S. Powell, 2017:   DYNAMO Legacy Rainfall Products. See Attachment 1.

Powell, S. W., R. A. Houze, and S. R. Brodzik, 2016: Rainfall-type categorization of radar echoes using polar coordinate reflectivity data. *J. Atmos. Oceanic Technol.*, **33**, 523–538, doi:10.1175/ JTECH-D-15-0135.1.

Attachment 1

DYNAMO Legacy Rainfall Products

B. Dolan, P. Hein, S. Rutledge, S. Powell

Assembled with input from S. Brodzik, E.Thompson, R. Houze, A. Funk, and W. Xu

(informally called the DYNAMO rain group)

bdolan@atmos.colostate.edu

In regards to the legacy DYNAMO data set for rainfall, we performed a number of studies to determine the optimal rainfall estimation equations, rain type classification, and uncertainty analysis. The uncertainty analysis lays out a methodology to assess uncertainty in the derived rain estimates due to uncertainties in the radar variables, assumed equations and rain type. It is important to state that without 'ground truth' for the rain estimates, it is impossible to assess the errors in application of the outlined algorithms to the radars, at least via traditional methods, such as by using available rain gauge data. This document describes the best methods for producing rain maps for the DYNAMO legacy data set.

Radar calibration

The S-Pol radar was calibrated with a full engineering calibration at the start of the project (gains, losses and transmit power). Solar scans were also performed. For Z, a self-consistency test was performed in rain for 3 periods, and a Z bias of <0.5 dB was determined in all cases. Z_{dr}, differential reflectivity, was calibrated using vertically pointing scans performed over 27 separate time periods. The mean bias was removed and the standard deviation of Z_{dr} was 0.1 dB. We assume that Z was calibrated to within 0.5 dB and Z_{dr} to within 0.1 dB for DYNAMO. K_{dp} was calculated using the Hubbert and Bringi (1995) FIR filter with 10 range bins (1.5 km with 150 m gate spacing) to limit smoothing. As shown by Bringi and Chandrasekar (2001), the error in the measurement of K_{dp} is dependent on the path over which it is calculated, which is a function of the number of samples and the gate size over that path length. Based on Fig. 6.35 in Bringi and Chandrasekar (2001) and using a path length of 1.5 km (10 gates and 150 m gate spacing), the standard deviation of K_{dp} for S-pol is taken as 0.8 deg km^{-1}.

The Mirai data was calibrated using ZAUTO (an automated calibration utility utilizing a test signal generator). These calibrations can be made available as needed. The data were also compared to TRMM/PR V7 and found to have no notable offset.

The Revelle radar was calibrated using solar gain calibrations on 9/27, 10/1, 10/4, 10/20, 11/6, 11/11 (2011), which consistently demonstrated a 1.5 dB "hot" bias. TRMM PR comparison (typical uncertainty 1-1.5 dB, Anagnostou et al. 2001) was also consistent with this offset. Therefore the Revelle Z values were uniformly decreased by 1.5 dB.

Gates with reflectivity but bad velocity data were removed to filter second-trip and RF noise in the Revelle and Mirai data. While sea clutter was typically not a problem, it was removed by evaluating successive sweeps at every ray/gate, and if the reflectivity echo within 75 km range remains below 2 km, the echo was deleted (this also has the effect of removing all echo within 5-8 km of the radar). This method was developed specifically to account for the behavior of sea clutter noted in this dataset.

The SMART-R radar reflectivity was "calibrated" using the most up-to-date version of TRMM PR overpasses during the period, yielding a bias of -4.0 dB with an uncertainty of +/- 1 dB. This offset also produced consistent results when compared with S-Pol data with matched resolution, interpolation scheme, and sectors. No solar gain calibrations were done for SMART-R.

The SMART-R dataset censors data to the west of the radar site, some of which is marginal in quality owing to the unintentional tilt of the radar platform. Before gridding, only rays moving clockwise from 338 degrees to 158 degrees were retained with the remaining rays censored. This helps remove some of the lower quality data to the west that suffered from ground/sea clutter.

Attenuation Correction

The three C-band radars were corrected for gaseous and rain attenuation. The gaseous attenuation correction is applied using an established C-band one-way attenuation value of 0.008 dBZ km^{-1} (maximum 150-km two-way correction of +2.4 dBZ). The rain attenuation correction method utilizes a direct relationship between A_h and Z. The relationship is based on 2 years of seasonal disdrometer data from Manus that was processed by E. Thompson (2014). The relationship for the 2-way attenuation is:

$$A_h = (9.294 \times 10^{-6} \text{ km}^{-1})Z^{0.879} \qquad \text{db/km} \tag{1}$$

The attenuation correction is not applied above the assumed freezing level (5.0 km).

Gridding

All radar data were gridded to 1 km in horizontal dimensions, and 0.5 km vertical spacing, centered on the individual radar using the RadX gridding software package. The rain maps are generated using data at 2.5 km above MSL.

Rainfall Equations

Thompson et al. (2015) undertook a detailed objective analysis of 2DVD data in the tropical, oceanic regime to determine the optimal relationship between reflectivity and rain rate (Z-R), and Thompson et al. (2017) derived relationships between dual-polarization observables and rain rate. The equations were derived using orthogonal minimization from long-term observations (18 months) at Manus Island, which was found to be nearly identical to the Gan Island short-term (~ 5 months) observations during DYNAMO (2)-(7):

Convective rain R(Z)$_c$:	$Z = 126\ R^{1.46}$	(2)
Stratiform rain R(Z)$_s$:	$Z = 291\ R^{1.55}$	(3)
All rain R(Z)$_a$:	$Z = 216\ R^{1.3}$	(4)
R(K_{dp}, Z_{dr}):	$R = 96.57\ K_{dp}^{0.93}\ Z_{dr}^{-2.11}$	(5)
R(Z_h, Z_{dr}):	$R = 0.0085\ Z_h^{0.92}\ Z_{dr}^{-5.24}$	(6)
R(K_{dp}):	$R = 56.04\ K_{dp}^{0.80}$	(7)

Note the linear forms of reflectivity ($Z_h = 10^{(dbz/10.)}$) and differential reflectivity Z_{dr} ($Z_{dr} = 10^{(Zdr/10.)}$) are used in these equations. Thresholds of $K_{dp} > 0.3$ deg km^{-1} and $Z_{dr} > 0.25$ dB were applied to develop the fits. As shown by Thompson et al. (2015), in the tropical oceanic environment of the DYNAMO experiment, dual Z-R relationships (2) and (3) for convective and stratiform rain are necessary because convective and stratiform rain possess distinct drop size distributions (DSDs). Eqn. (4) represents a fit to all the data with no distinction for convective and stratiform rain. Performance of these equations compared to other relationships, such as the one derived from the MISMO experiment (Oct-Dec, 2006), were studied and found to produce the most accurate results in terms of convective and stratiform rainfall statistics when compared against the 2DVD-derived rainfall statistics [Table 8 in Thompson et al. (2015)]. MISMO was found to lean toward the convective DYNAMO relationship, likely due to the more convective sampling during that project (only one MJO episode was observed versus three MJO events during DYNAMO). *Thus, the Thompson et al. (2015) relationships (2)-(4) represent the best rainfall relationships for application to the DYNAMO single-polarization radar data. Hence these relationships will be utilized for the DYNAMO Legacy Data rain rate maps.*

Thompson et al. (2017) found that the dual-polarization-based relationships (5)-(7) are better correlated to 2DVD derived rain statistics compared to Z-R (Table 1). A tropical, blended algorithm was designed to maximize usage of the dual-polarization data while minimizing the uncertainty in rain rate associated with measurement error. The resulting algorithm is based on calculation of an initial rain rate using the R(Z)$_a$ relationship, then selecting the R(Z_h,Z_{dr}) algorithm when the rain rate is between 10 and 85 mm h^{-1}, and allowing the R(Z_{dr}, K_{dp}) formulation at rain rates > 85 mm h^{-1}. Thresholds on Z_{dr} and K_{dp} are also imposed to ensure the best quality in the measurements; below these thresholds dual Z-Rs are used. *Thus, application of the CSU blended rainfall logic with updated equations, including dual Z-Rs in the R(Z) branch (Fig. 1), represents the best rainfall estimation methodology for application to the S-Pol radar during DYNAMO. This methodology will be adopted for use in producing the S-Pol based rain maps.* For the single-polarization C-band radars, the logic outlined in the subset box in Fig. 1 is applied, utilizing the dual-Z-R relationships.

Table 1: S-band dual-polarization relationships derived from 2DVD over the tropical, oceanic regime. Separate convective/stratiform equations refer to the Thompson et al. (2015) partitioning method [Adapted from Thompson et al. (2016)]. Correlation coefficients between 2DVD derived rainfall and

rainfall estimated using Eqns. (2)-(7) with 2DVD synthetic S-band dual-polarization observations are in the second column.

| Rain Estimation Equation	Correlation Coefficient
Convective rain $R(Z)_c$ Stratiform rain $R(Z)_s$	0.967
All rain $R(Z)_a$	0.925
$R(K_{dp}, Z_{dr})$	0.996
$R(Z_h, Z_{dr})$	0.992
$R(K_{dp})$	0.988
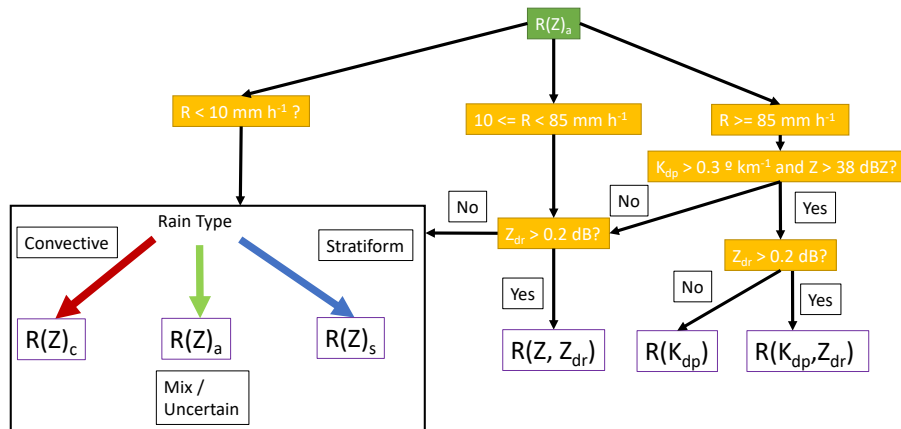
Figure 1: Rainfall estimation logic for "CSU tropical, oceanic blended algorithm" for application in DYNAMO. Single-polarization radars use the subset box on the left.

Rain Typing

A rain typing algorithm by Powell et al. (2016, hereafter PHB16) accounts for the ubiquitous shallow, weak convection prominent in the DYNAMO region. The PHB16 rain typing includes six categories:

Stratiform
Convective
Mixed
Isolated convective core (ICC)
Isolated convective fringe (ICF)
Weak echo

We tested several thresholds for the reflectivity threshold for convection (Z_{th}) and the minimum reflectivity for the convective core radius (Z_{conv}) parameters within PHB16 algorithm, and found that for the Revelle and Mirai (C-band, 1.5º beam width), the most physically-reasonable convective/stratiform classification (compared with subjective eye determination of convective areas) was achieved with Z_{th} = 36 dBZ and Z_{conv} = 41 dBZ. For SMART-R, thresholds of 38 /43 for Z_{th} and Z_{conv} were used, which were found to give the best match for rainfall volume fractions compared to the other radars. The Z_{th} threshold (36 dBZ) represents the 95th percentile of reflectivities in the 1 km gridded data set and best reproduces the 2DVD-derived convective/stratiform rain volume contributions [assuming as a first estimate that 'mixed' echoes take the classification they would have received by running the convective/stratiform classification algorithm of Steiner et al. (1995)]. We performed several sensitivity studies in order to understand how to best apply the rain estimators, including treating the mixed category and ICF as convective or stratiform, and applying the single $R(Z)_a$ to the mixed category (Table 2). Here we use the 2DVD derived convective/stratiform fraction of 81/19 as the anchor to compare rain volume percentages against (Thompson et al. 2015). In a separate test, we determined that the 'mixed' category has approximately 50/50 convective/stratiform areal occurrence (although in terms of rain volume, this category has larger contributions from convective rain), indicating that the single Z-R is the most applicable relationship. Analysis of the S-Pol radar signatures associated with the isolated convective fringe category suggest the shape and size of hydrometeors look very much like stratiform, and, therefore, $R(Z)_s$ should be applied. This treatment of Z-R relationships for the PHB16 rain type categories resulted in the most similar rain volume statistics to the 2DVD (yellow column, Table 2). Application of this same configuration to the Mirai radar data resulted in similar statistics (Table 3), with a slightly higher percentage of convection in frequency of occurrence and contribution to total rain volume. *Thus, for application to the DYNAMO radars, the convective, ICC, and weak echo categories use $R(Z)_c$; stratiform and ICF employs $R(Z)_s$; the single $R(Z)_a$ is used for the mixed category.*

Table 2: Sensitivity study for application of the Z-R relationships for PHB16 rain type categories as applied to the Revelle DYNAMO cruise 2-4. Columns 2-5 are rain volume percentages.

Rain Type	Mixed with $R(Z)_c$	Mixed with $R(Z)_s$	Mixed with single $R(Z)_a$	Mixed with single $R(Z)_a$ and ICF with $R(Z)_s$	Rain Area Percent Occurrence
Convective	47	54	50	52	6
Stratiform	11	12	11	12	41
Mixed	26	16	21	22	20
Isolated Convective Core	8	9	8	9	3
Isolated Convective Fringe	8	9	9	5	21
Weak Echo	~0	~0	~0	~0	8
Total Convective:	63	72	67	61	17

| Total Stratiform: | 11 | 12 | 11 | 17 | 62 |
| Total Mixed: | 26 | 16 | 21 | 22 | 20 |

Table 3: Statistics from application of the PHB16 algorithm and R(Z) application as in Table 2 (yellow column) to the Mirai data.

Rain Type	Mixed with single $R(Z)_a$ and ICF with $R(Z)_s$	Rain Area Percent Occurrence
Convective	55	6
Stratiform	7	28
Mixed	21	21
Isolated Convective Core	9	4
Isolated Convective Fringe	7	31
Weak Echo	1	11
Total Convective:	65	21
Total Stratiform:	14	59
Total Mixed:	21	21

Uncertainty and Error Analysis

Without absolute truth, it is impossible to assess the error in the rainfall estimates. *Instead we choose to examine the uncertainty associated with error in the radar measurements and error associated with the derived rain rate formulations*. First, it is important to consider the impact of choosing a single Z-R estimator, like the MISMO relationship vs. using the new dual Z-R estimators. As summarized in Table 8 of Thompson et al. (2015), using a single Z-R instead of a dual Z-R approach results in a +/-10% difference in convective/stratiform rain fractions. Although application of the MISMO single-relationship results in small difference in total rainfall accumulation, it leads to significant differences in the contributions from stratiform and convective rain by overestimating stratiform rain by 58% (because the MISMO fit line is skewed toward convective rain). Similarly, applying different dual-polarization rainfall optimization algorithms results in small differences to the overall accumulated rain and convective/stratiform rain fractions. Application of different Z-R relationships (such as convective or stratiform) to the mixed PHB16 rain type changes the overall convective rain volume fraction by ~9%. Therefore, a dual Z-R formulation is utilized, with distinct Z-R's for convective and stratiform rain types. In order to account for the uncertainty associated with the 'mixed' category, the minimum (maximum) rain maps will treat the mixed category as stratiform (convective).

The total error in rain rate is the sum of the error due to the rain rate estimator formulation and measurement error. We define these as the root mean square error of the fit, RMSE, and the normalized standard deviation due to measurement error, $\sigma(\varepsilon_m)$:

$$\sigma_{tot} = \sigma(\varepsilon_m) + RMSE$$

(8)

Measurement Uncertainties

Despite good calibration, random sampling error remains in the radar measurements. Following Bringi and Chandrasekar (2001), a standard deviation is used to account for this random error for all radars, where 0.8 dB is used for reflectivity and 0.2 dB for Z_{dr}. The uncertainty in K_{dp} is highly dependent on the path length over which it is estimated. We assume the path length is 1.5 km and the gate spacing is 150 m, as was used for the S-Pol data set, and we use Fig. 6.35 from Bringi and Chandrasekar (2001) to arrive at a value of 0.8 deg km^{-1} for the standard deviation of K_{dp}.

Following Bringi and Chandrasekar (2001) Section 8.3, $\sigma(\varepsilon_m)$, the normalized standard deviation due to measurement error, can be estimated for each radar rainfall estimator.

R(Z): $$\frac{\sigma(\varepsilon_m)}{R} = a\frac{\sigma(Z)}{Z}$$ (9)

R(K_{dp}): $$\frac{\sigma(\varepsilon_m)}{R} = a\frac{\sigma(K_{dp})}{K_{dp}} = a\sigma(K_{dp})\left(\frac{c}{R}\right)^{(1/a)}$$ (10)

R(Z,Z_{dr}): $$\frac{\sigma(\varepsilon_m)}{R} = \sqrt{a^2\frac{\sigma(Z)^2}{Z^2} + b^2\frac{\sigma(Z_{dr})^2}{Z_{dr}^2}}$$ (11)

R(K_{dp},Z_{dr}): $$\frac{\sigma(\varepsilon_m)}{R} = \sqrt{a^2\frac{\sigma(K_{dp})^2}{K_{dp}^2} + b^2\left(\frac{\sigma(Z_{dr})^2}{Z_{dr}^2}\right)}$$ (12)

where $\sigma(Z)$, $\sigma(Z_{dr})$, $\sigma(K_{dp})$ are the standard deviations in the measurements, and a and b are the exponents of the rain rate relationships in (2)-(7). The variable c in (10) is the coefficient from (7). The coefficients and values used to establish measurement error as a function of rain rate are given in Table 4, and are plotted as $\sigma(\varepsilon_m)/R$ in Fig. 2. We also note that the power-based measurement (Z and Z_{dr}) errors, there is a constant relationship between the measurement error ($\sigma(Z)$) and the measured reflectivity Z (where Z is in dB), such that $\sigma(Z)/Z = 0.2$ if the reflectivity measurement error is 0.8 dB, and $\sigma^2(Z_{dr})/Z_{dr}^2 = 0.0022$ for an assumed error of 0.2 dB in Z_{dr}. Therefore, the measurement uncertainty, $\sigma(\varepsilon_m)/R$, is also a constant value invariant with rain rate (Table 5, Eqn. 9,11). On the other hand, $\sigma^2(K_{dp})/K_{dp}^2$ follows a 1/R curve, where R is the rain rate (Eq. 10).

Table 4: Coefficients and values used in (9)-(12) to estimate the error due to measurement uncertainty.

	a	b	$\sigma(Z)$	$\sigma(Z_{dr})$	$\sigma(K_{dp})$
$R(Z)_a$	0.721	--	0.8	--	--
$R(Z)_c$	0.684	--	0.8	--	--
$R(Z)_s$	0.644	--	0.8	--	--
$R(K_{dp})$	0.825	--	--	--	0.8
$R(Z,Z_{dr})$	0.924	-5.239	0.8	0.2	--
$R(K_{dp},Z_{dr})$	0.932	-2.114	--	0.2	0.8

Table 5: $\sigma(\varepsilon_m)/R$ values for R(Z) and R(Z,Z_dr).

	$\sigma(\varepsilon_m)/R$
$R(Z)_a$	0.144
$R(Z)_c$	0.137
$R(Z)_s$	0.129
$R(Z,Z_{dr})$	0.307
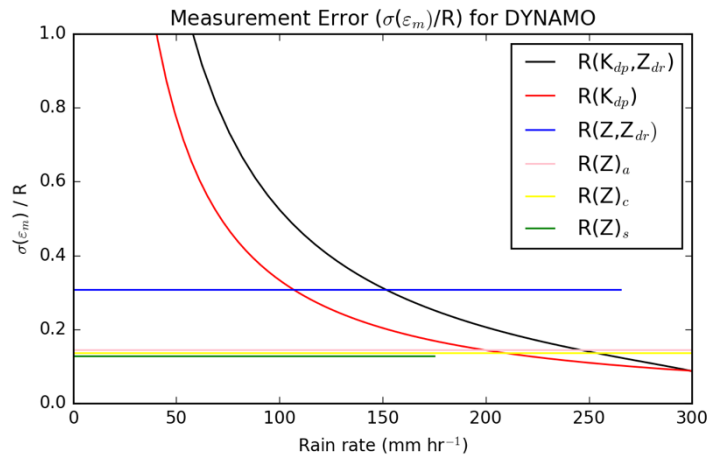
Figure 2: The normalized standard deviation for the measurement error associated with each radar rainfall relationship assuming (9)-(12) and the values in Table 5 for S-Pol (Note: these lines have been generated using assumed linear relationship between Z-Z_{dr} and Z_{dr}-K_{dp} for the purpose of illustration). Bringi and Chandrasekar (2001) note that in order to compare the relationships using K_{dp} to the power-based relations, a factor of $1/\sqrt{N}$ should be applied where N is the number of gates used to calculate K_{dp}.

Rain Rate Equation Fitting Uncertainties

To account for errors in the assumed relationship between radar variables and rain rate, the root mean square error (RMSE) for each relationship was calculated in three size bins: 1 mm h^{-1}, 5 mm h^{-1}, and 10 mm h^{-1}. [These tables can be provided as needed]. Then a curve was fit to RMSE vs. R to form a relationship (Fig. 3). Given the number of points for each bin, three different fits are used based on rain rate thresholds. For R<20 mm h^{-1} (<10 mm h^{-1} for stratiform), a fit to the 1 mm h^{-1} bins is used; for $20 \leq R < 60$ mm h^{-1} ($10 \leq R < 20$ for stratiform) the 5 mm h^{-1} bin fit is used, and for R > 60 (R > 20 mm h^{-1} for stratiform) a fit to the coarse 10 mm h^{-1} is used. The relationships are in the form:

$$RMSE = AR^B \qquad\qquad (13)$$

and coefficients are given in Table 6. The overall fit curves are plotted in Fig. 4.

In order to capture spatial and temporal variability in the instantaneous rainfall uncertainty, we establish minimum and maximum rain rate estimates based on the measurement and fit uncertainty. Regardless of the Z-R relationship used to determine a value of R at a given grid point, the maps of the maximum (minimum) values are generated by adding (subtracting) to (from) R the values of $\sigma(\varepsilon_m)$ [from Equations (9)-(12) using values in Table 5] and 2*(RMSE) [from Equation (13) using values in Table 6]. An example of the approximate minimum and maximum rain rates due to the total error (measurement + rain rate formulation, Eqn. 8) are illustrated in Fig. 5.
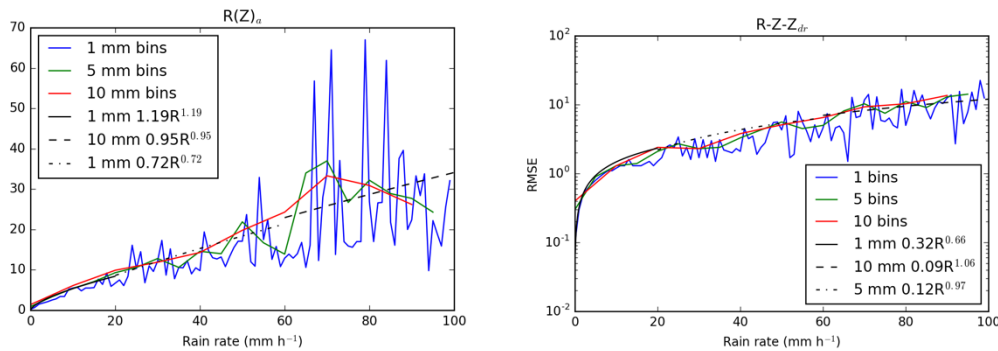

Fig. 3: Example of RMSE vs. Rain rate for 1, 5 and 10 mm h^{-1} bin sizes, and the approximate fitted curves for the case of (left) single Z-R and (right) R-Z-Z$_{dr}$.

Table 6: Coefficients for the error associated with the rain rate estimator fit. Here <20 indicates the coefficients are applied when the rain rate is < 20 mm h^{-1}.

RMSE	A (<20)	B (< 20)	A (<=20 R<60)	B (<=20 R<60)	A (>60)	B(>60)
R-Z All	1.19	0.65	0.72	0.83	0.95	0.78

R-Z$_c$	0.49	0.80	0.21	1.08	0.3	1.0
R-Z$_s$	(<=10)	(<=10)	(10<R<=20)	(10<R<=20)	(>20)	(>20)
	0.78	0.62	0.82	0.68	0.76	0.78
R-K$_{dp}$	0.88	0.57	0.63	0.70	0.75	0.67
R-Z-Z$_{dr}$	0.32	0.66	0.12	0.97	0.09	1.06
R-K$_{dp}$-Z$_{dr}$	0.73	0.38	0.77	0.37	0.94	0.32
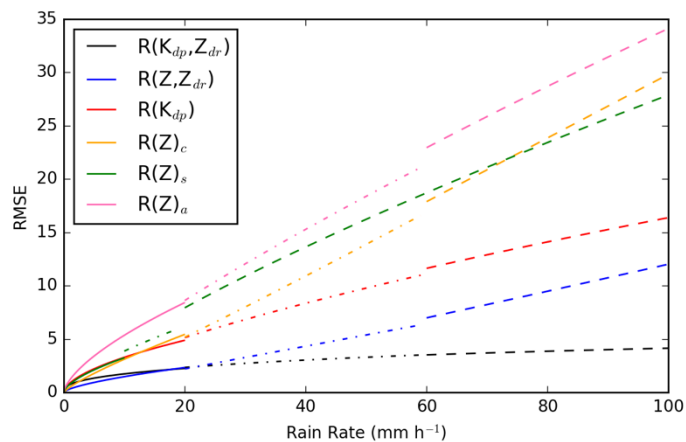
Figure 4: RMSE as a function of rain rate from (12) with coefficients given in Table 6. Dashed line indicate the fit for R > 60 mm h^1 (R > 20 mm h^{-1} for stratiform), and the dash-dot for $20 \leq R < 60$ mm h^{-1} ($10 \leq R < 20$ mm h^{-1} for stratiform).
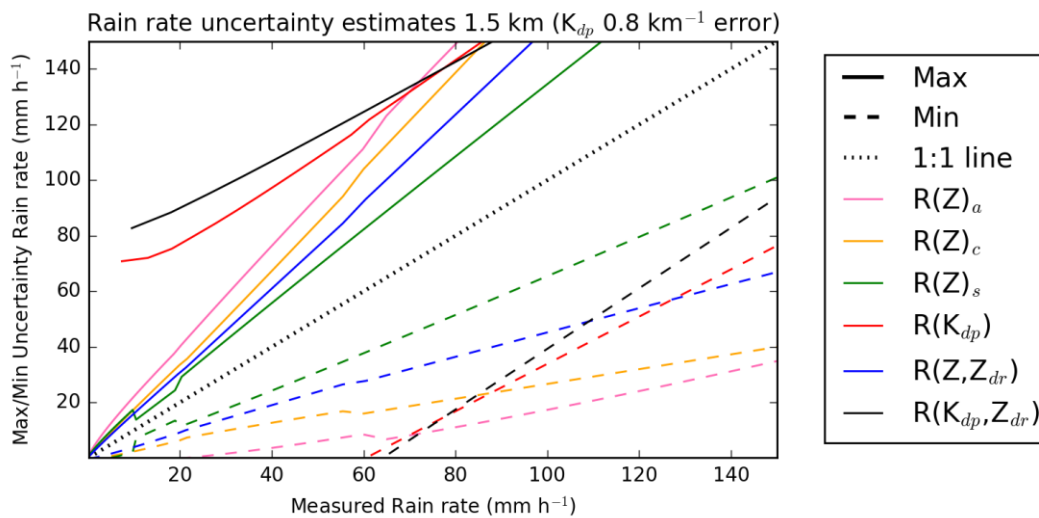

Figure 5: Minimum and maximum rain rates as a function of rain rate based on uncertainty analysis accounting for errors in measurements and rain rate fits.

Lastly, to account for uncertainty in the handling of the 'mixed' category in the rain typing algorithm, we applied R(Z)$_s$ to the mixed category to generate the minimum rain rate map and R(Z)$_c$ to generate the maximum rain rate map. We note here that the instantaneous rain rate uncertainty is extremely large at any given point. However, spatial and temporal averaging significantly decreases the uncertainty in the rain estimates.

Final Products

Based on interpolated moments at 2.5 km above MSL , with 1 km^2 horizontal resolution

<u>C-band, single Pol radars</u>:

> Rain rate at each grid point using PHB16 rain type, Z-Rs from Thompson et al. (2015) (lower box in Fig. 1)
> Uncertainty rain rate maps (Fig. 6)
> Maximum: add ($\sigma(\varepsilon_m)$ + 2*RMSE) for given rain rate and specific rain estimator, apply Z-R$_c$ to the mixed category points
> Minimum: subtract ($\sigma(\varepsilon_m)$ + 2*RMSE) for given rain rate and specific rain estimator, apply Z-R$_s$ to the mixed category points

<u>S-Pol</u>

Rain rate from CSU 'tropical' blended algorithm (defined in Fig. 1)

Method/rain rate estimator used to compute rain rate from CSU 'tropical' blended algorithm

Uncertainty rain rate maps (Fig. 6)

Maximum: add [$\sigma(\varepsilon_m)$ + 2(RMSE)] for given rain rate and specific rain estimator, apply Z-R$_c$ to the mixed category points

Minimum: subtract [$\sigma(\varepsilon_m)$ + 2(RMSE)] for given rain rate and specific rain estimator, apply Z-R$_s$ to the mixed category points
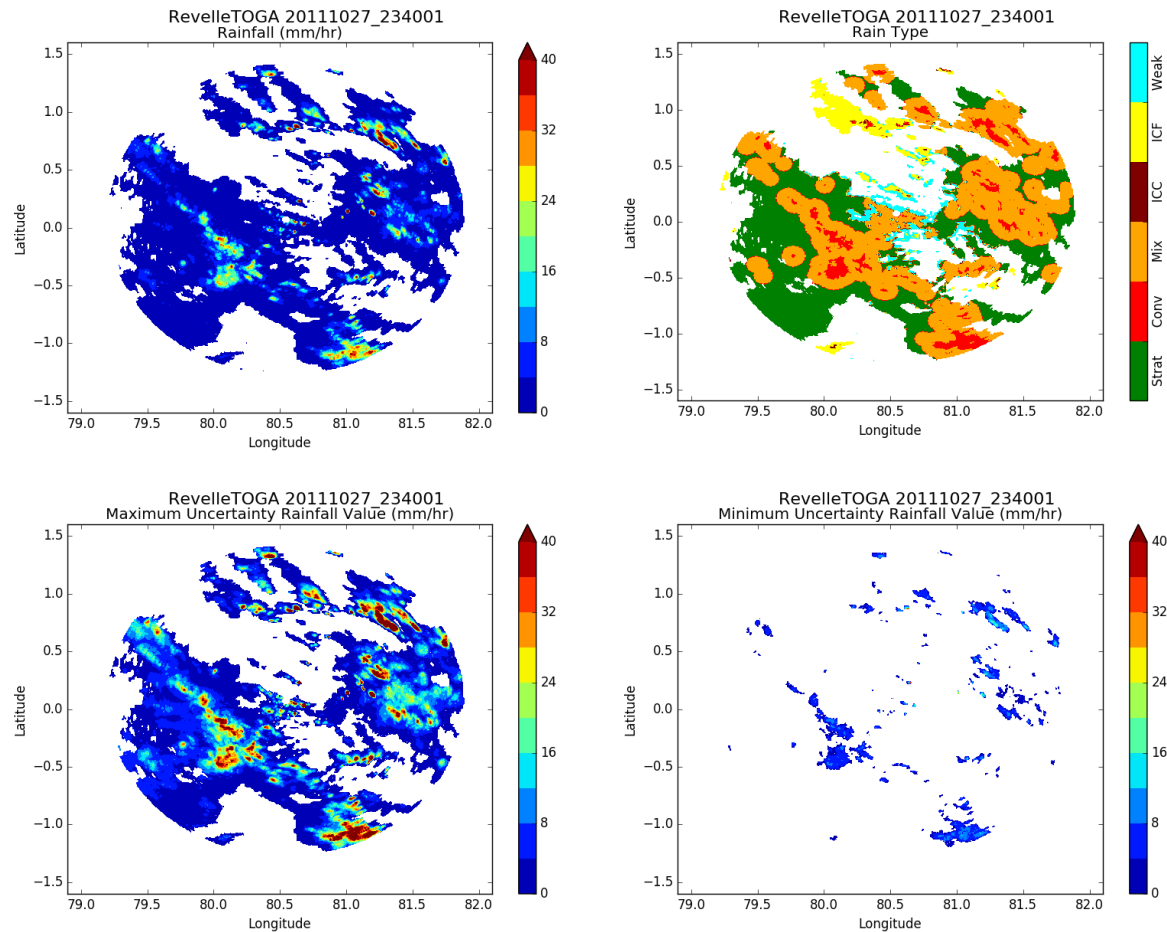
Figure 6: Example products from the Revelle radar. Rain rate best estimate (upper left), rain type (upper right), maximum rain rate (lower left), minimum rain rate (lower right).

References

Bringi, V. N. and V. Chandrasekar, 2001: *Polarimetric Doppler Weather Radar: Principles and Applications*. Cambridge University Press, Cambridge, United Kingdom, pp. 636 pp.

Hubbert, J., and V. N. Bringi. "An iterative filtering technique for the analysis of copolar differential phase and dual-frequency radar measurements." *Journal of Atmospheric and Oceanic Technology* 12.3 (1995): 643-648.

Powell, S. W., R. A. Houze, and S. R. Brodzik, 2016: Rainfall-type categorization of radar echoes using polar coordinate reflectivity data. *J. Atmos. Oceanic Technol.,* **33**, 523–538, doi:10.1175/ JTECH-D-15-0135.1.

Steiner, M., R. A. Houze Jr., and S. E. Yuter, 1995: Climatological characterization of three-dimensional storm structure from operational radar and rain gauge data. *J. Appl. Meteor.*, **34**, 1978–2007, doi:10.1175/1520-0450(1995)034,1978: CCOTDS.2.0.CO;2.

Thompson, E. J., S. A. Rutledge, B. Dolan, M. Thurai, and V. Chandrasekar, 2017: Dual-polarization radar rainfall estimation over tropical oceans. *J. Appl. Meteor.*, in preparation.

Thompson, E. J., S. A. Rutledge, B. Dolan, and M. Thurai, 2015: Drop size distributions and

radar observations of convective and stratiform rain over the equatorial Indian and West Pacific Oceans. *J. Atmos. Sci.* **72**, no. 11 (2015): 4091-4125.

Zrnic D.S., V. M. Melnikov, and J. K. Carter, 2006: Calibrating differential reflectivity on the WSR-88D. *J. Atmos. Ocean. Technol.*, **23**, 944-951.